JOURNAL OF THE TAIWAN INSTITUTE OF CHEMICAL ENGINEERS 85 (2018): 66-73

DOI: https://doi.org/10.1016/j.jtice.2017.12.015

*

Optimization of Disperse Blue 3 mineralization by UV-LED/$FeTiO_3$ activated persulfate using response surface methodology

Jefferson E. Silveira[1*], Elis Marina Turini Claro[2], Adriana S. Oliveira[1], Wendel S. Paz[1], Juan A. Zazo[1], Jose A. Casas[1]

[1]Chemical Engineering, Autonomous University of Madrid, Cantoblanco, 28049 Madrid, Spain

[2]São Paulo State University (UNESP), Institute of Biosciences, Department of Biochemistry and Microbiology, Av. 24 A, 1515, Bela Vista, Postal Code 13506-900 - Rio Claro, SP, Brazil.

*Corresponding author. Tel.: +34 914972487

E-mail address: jeffersonan@gmail.com

ABSTRACT

Response surface methodology based on Box-Behnken Design (BBD) design was successfully applied to the optimization in the operating conditions of the UV-LED/$FeTiO_3$ activated persulfate (PS). Disperse Blue 3 (DB3) azo dye was treated in a glass jacketed batch reactor using external UV radiation at 405 nm with radiation of 10W m^{-2}. The effects of three variables, temperature reaction, ilmenite concentration and persulfate stoichiometric amount upon the total organic carbon (TOC) removal were evaluated. Optimized conditions were obtained for the highest desirability at 320 mg L^{-1} of ilmenite using 92% of stoichiometric amount of PS at 67 °C under UV-LED radiation. Under the optimal conditions, 96% of total organic carbon (TOC) removal was achieved, being the ecotoxicity of the effluent almost negligible to the Aliiv*ibrio fischeri* bacteria.

Keywords: Optimization, Box-Behnken Design, $FeTiO_3$, photo-reduction

1. Introduction

The continuously demographic growth and the steep expansion of the industrial sector constitute an increasing pressure over the water sources due to uncontrolled discharge of effluents that contribute to an irreversible reduction in fresh water availability [1]. The synthetic dyes industry can be considered as a representative example, which raw effluents could contain recalcitrant and potentially carcinogenic compounds due to the nature of its organic molecules [2].

Nowadays, over 100.000 different dye structures have been synthesized and more than 0.7 million tons of dyestuff with applications in textile, paper, leather, cosmetics, food or pharmaceutical industries are produced annually [3,4]. Worldwide, 280.000 tons of textile dyes are discharged in industrial effluents annually [5]. Among the different types, azo dyes are the largest group of dyes used in textile dyeing and printing industries, since they account for about 70% of the world dye production. These dyes belong to the class of aromatic and heterocyclic compounds contain an azo group (-N = N-) as chromophore, linked to other groups such as - OH and -NO_2[6,7].

Therefore, the azo dyes are difficult to remove through traditional treatment methods because of their complex structure and high stability and chromaticity, which justifies the need for more effective water treatment technologies [8]. Advanced oxidation processes (AOPs), which relies primarily on the generation of the free radicals to degrade organic compounds have shown great potential. Advance techniques are used for the activation of the oxidants and thus provide a clean way of generating highly oxidizing radical species [9].

Recently, sodium persulfate (PS) anion has emerged as a promising emerging oxidant, which are also utilized in azo dye treatment [10]. The PS presents high solubility, high stability and wide operative pH range in aqueous solution, however, reactions of PS with organic substance in water are generally slow at ambient temperature, therefore it is necessary

to activate PS generating a stronger sulfate radical ($SO_4^{\bullet-}$), with a standard redox potential varying between 2.5 V and 3.1 V, to accelerate the degradation rate of organic compound [8,11]. Generally, activation of persulfate can be accomplished by a transition metal ion which acts as a catalyst, usually Fe(II). Because Fe is relatively non toxic and inexpensive among various transition metal catalysts, it has been widely studied to activate persulfate oxidation for contaminant removal [12]. Several types of Fe-based catalysts in different AOPs processes, were used for the chemical activation of persulfate, including the polycrystalline $FeTiO_3$ (natural ilmenite) [13]. Ilmenite is a antiferromagnetic semiconductor, with a band gap varying between 2.3 and 2.9 eV with potential applications in chemical catalysts reactions [14].

The high induction period and lower activity, due to a high electron-hole recombination represents one of the main drawbacks of this mineral catalyst [14]. This problem can be solved by using UV irradiation to improve the efficiency via photoreduction of Fe(III) to Fe(II) in the ilmenite surface, decreasing the induction period [15]. In addition, Cheng et al. [16] and Bokare and Choi [17] suggest that in the presence of colored substances like organic dyes, visible light irradiation can also reduce Fe(III) to Fe(II) via intermolecular electron transfer from an excited dye state, Eq. 1-3 and enhance the generation of $SO_4^{\bullet-}$ and $HO^{\bullet}$.

$$\text{ILM - Fe(III)} \xrightarrow{v} \text{ILM - Fe(II)} \quad \textbf{(1)}$$

$$\text{dye} + \text{visible light} \rightarrow \text{dye}^{*} \quad \textbf{(2)}$$

$$\text{dye}^{*} + \text{Fe(III)} \rightarrow \text{Fe(II)} + \text{dye}^{\bullet+} \quad \textbf{(3)}$$

Ultraviolet light emitting diodes (UV-LEDs) are a promising source of UV radiation and become an alternative to photocatalysis reactions, with the potential advantages over

conventional UV lamps such as instant on/off ability, tunable radiation to control the peak wavelength, compactness, long life and minimal disposal problems increases the flexibility of photoreactor designs [18–21].

In this sense, this work outlines the operating variables such as persulfate stoichiometric amount, ilmenite concentration and temperature reaction under UV-LED radiation monitored by TOC removal and PS consumption toward of azo dye Disperse Blue 3 (DB3) mineralization in order to optimize the process. Box-Behnken design (BBD), a type of response surface methodology (RSM), and the empirical models the variables were developed. The acute toxicity of the solutions was evaluated before and after treatment using *Aliivibrio fischeri*.

2. Material and Methods

2.1. Materials

Azo dye DB3was obtained from Sigma-Aldrich and their characteristics are presented in Table S1.

All chemicals used in the experiments were analytical reagent grade. Potassium iodide (KI - 99.0%), sodium carbonate (Na_2CO_3 – 99.0%), sodium bicarbonate ($NaHCO_3$ – 99.7%), sodium sulfate (Na_2SO_4 – 99.0%) and dichloromethane (CH_2Cl_2– 99.8%) was purchased from Sigma-Aldrich (Milwaukee, WI, USA). Sodium persulfate ($Na_2S_2O_8$ – 98.0%) was obtained from PanReac AppliChem (Barcelona, Spain). The natural ilmenite (Ref. 50110700) was provided by Marphil S.L. (Spain). Table 1 summarizes the main physico-chemical properties of natural ilmenite. For the sake of comparison, this table also includes the Fe(III)/Fe(II) ration of ilmenite after photo-reduction with and without DB3.

Table 1. Physico-chemical properties of ilmenite.

Ilmenite/Rutile phases (%)	S_{BET} (m^2g^{-1})	$Fe(III)/Fe(II)_{surface}$			Band-gap value (eV)
		Natural ilmenite	Photo reduced	Photo/ Dye reduced	
85/15	6	58/42	52/48	30/70	2.4

2.2. Catalytic oxidation procedure

The reactor in glass jacketed batch (usable volume: 250 mL) equipped with a magnetic stirrer (Fig. S1) was built to evaluate the catalytic activity. A commercial LED strip (SMD 5050), λ = 405 nm, with radiation of 10 W m^{-2} and a power of 19 W, was placed around the external wall of the reactor. In all cases, 80 mg L^{-1} DB3 was used as initial concentration at pH 3 using concentrated H_2SO_4. The temperature was controlled between 30-70 ˚C with a thermal batch recirculation system (Julabo 13). Experiments were carried out after adding a known amount of PS (1.7 g L^{-1} or 100%) that correspond to the stoichiometric amount needed for DB3 mineralization and substoichiometric amount varying between 20% (0.34 g L^{-1}) and 60% (1.02 g L^{-1}) and ilmenite concentrations ranged between 150 and 450 mg L^{-1}, to match chosen experimental range and levels of independent variables (Table 2). The exposure time of mixture was 180 min and samples were taken afterward for analysis and were instantly placed in an ice bath and immediately analysed after centrifugation (Digicen 21) at 5.294 x *g* for 10 min. All experiments were performed in triplicate.

2.3 Analysis procedure and toxicity testing method

Decolorization extents were obtained by measuring the absorbance in visible spectra at the characteristic maximum wavelength (λ_{max}= 640 nm) by using a UV-VIS spectrophotometer (Agilent Cary 60). The mineralization of DB3 solution was established on

the performed by using a TOC analyzer (TOC-V CSH, Shimadzu, Japan). The concentration of PS was monitored spectrophotometrically (λ_{max}=352 nm) by a modified iodometric titration method [22]. The total iron content released from the ilmenite was measured by Inductively Coupled Plasma Optical Emission Spectroscopy (ICP-OES) using an ICP-MS Elan 6000 PerkinElmer Sciex instrument. Ilmenite was characterized by X-ray Photoelectron Spectroscopy (XPS) with a Kα Thermo Scientific apparatus with an Al Kα (hv=1486.68 eV) X-ray source using a voltage of 12 kV under vacuum (2×10^{-7} mbar) condition. For the peak analysis, a Shirley type background was used. Peaks were fitted with Gaussian and Lorentzian functions using the XPS Peak 4.1 software [23].

Degradation products were detected by mass spectra and their fragmentation pattern. For this, a gas chromatography coupled with a mass spectrometry (GC-MS) was used (CP-3800/Saturn 2200, Varian) and was performed liquid-liquid extraction, using 5 mL of the initial or mineralized DB3 and extracted with dichloromethane (15 mL) in three times and the sample was preconcentrated by evaporation at 40 ºC. The by-product 1-amino-4-(methylamino) anthracene-9,10-dione with m/z 252 was identified using the National Institute of Standards and Technology (NIST) database. A more detailed analytical methodology were described elsewhere [24].

Toxic effects of DB3 after the treatment was evaluated using a commercially available bio-test (MicroTox®) based on reduction of bio-luminesce of aquatic bacteria *A.fischeri*. Changes in bacteria concentration is sensed by means of natural bio-luminesce that is measured using a photometer [25]. The response established for the toxicity test with *A.fischeri* was the mean lethal concentration (EC_{50}) meaning the sample initial concentration which reduced 50% of the total biological effect (light emission). Once the results are inversely proportional the EC_{50} data was transformed to Toxic Units (TU) and was used to evaluate the toxicity of collected samples [26].

2.4. Response surface methodology experimental design

The model performance, might be expressed using a second-order polynomial equation (Eq. 4).

$$R = \beta_0 + \sum_{i=1}^{k} \beta_i x_i + \sum_{i=1}^{k} \beta_{ii} x_i^{\,2} + \sum_{i=1} \sum_{j=1+1} \beta_{ij} x_i x_j + \varepsilon \quad \textbf{(4)}$$

where: R is the predicted response for TOC removal, β_0 is the intercept parameter, β_i, β_{ii} *e* β_{ij} are parameters for linear, quadratic and interaction factor effects, X_i e X_j are independent variables and ε is the error. The number of experiments (N) required for the development of this design is defined as N=2k (k×1)+C_0, where k is the factor number and C_0 is the replicate number of the central point [27].

The experimental independent variables ilmenite concentration (A), persulfate stoichiometric dose (B) and reaction temperature (C) were analyzed at three levels, coded as −1, 0, and 1 (low, center and high) would be 27 (3^3), which has been reduced to15 experiments using BBD experimental design, summarized in Table 2, to get the DB3 mineralization.

Three-dimensional response surface plots were used to gain insight about the effect of each variable and interactive effects. The fit between the model and the experimental data was evaluated by ANOVA (analysis of variance). The F-test was applied to verify whether the model could predict a significant variation in the experimental data. The Probability *p* value was used to estimate whether F is large enough to indicate statistical significance [28]. The model was developed using the software Design Expert v.8.0.7.1.

Table 2. The BBD design matrix and experimental results.

Run	Actual Conditions	CodedFactors	TOC removal(%)	PS consumption(%)

	Ilmenite (mg L^{-1})	Persulfate (%)	Temperature (°C)	A	B	C	Exp	Pred	Exp	Pred
1	450	20	50	+1	-1	0	20	15.4	92	93.8
2	150	100	50	-1	+1	0	22	26.6	24	22
3	150	60	30	-1	0	-1	7	4.0	21	17
4	300	60	50	0	0	0	30	31.2	35	33
5	150	20	50	-1	-1	0	8	6.6	45	50
6	450	60	30	+1	0	-1	17	16.5	82	82
7	450	100	50	+1	+1	0	52	53.4	54	48
8	450	60	70	+1	0	+1	64	67.75	87	91
9	300	20	70	0	-1	+1	36	36.8	100	94.5
10	300	20	30	0	-1	-1	5	10	90	88
11	300	100	70	0	+1	+1	91	86	88	89.8
12	150	60	70	-1	0	+1	45	45.5	86	86
13	300	100	30	0	+1	-1	20	19.2	13	18
14	300	60	50	0	0	0	32	31.2	31	33
15	300	60	50	0	0	0	31.5	31.2	33	33

3. Results and Discussion

3.1 Box-Behnken analysis: model evaluation

The experimental matrix (Table 2) was conducted to establish a model to obtain the highest degree of DB3 mineralization. The accuracy of model fitting in the form of ANOVA (F-test and *p*) are displayed in Table 3. The ANOVA results confirm the significance of the model in each case along with its individual factor at the level of Prob>F less than 0.05.

The model F-values of 31.73 and 42.36 pointed out that it was significant at $p < 0.0007$ and 0.0003 respectively for TOC removal and PS consumption. Also, A, B, C, AC, BC, A^2, C^2 are significant model terms in TOC removal and A, B, C, AC, BC, A^2, B^2 and C^2 are significant terms in PS consumption. The adequate precision is a measure of the range in predicted response relative to its associated error, being desirable a signal-to-noise ratio greater than 4.0 [29].

Table 3. ANOVA test for TOC removal efficiency TOC and PS consumption.

SOURCE	Sum of Squares		Df	Mean square		F-value		p[a]-valueProb> F	
	TOC	PS		TOC	PS	TOC	PS	TOC	PS
Model	7,505.82	13,478.18	9	833.98	1,497.58	31.73	42.36	0.0007	0.0003
A	1,682.00	2,738.00	1	1,682.00	2,738.00	63.99	77.45	0.0005	0.0003
B	630.13	2,415.12	1	630.13	2,415.12	23.97	68.32	0.0045	0.0004
C	4,371.13	3,003.13	1	4,371.13	3,003.13	166.31	84.95	<0.0001	0.0003
AB	81.00	72.25	1	81.00	72.25	3.08	2.04	0.1395	0.2122
AC	400	1,056.25	1	400	1,056.25	15.22	29.88	0.0114	0.0028
BC	20.25	900.00	1	20.25	900.00	0.77	25.46	0.4202	0.0039
A^2	0.78	554.08	1	0.78	554.08	0.030	15.67	0.8703	0.0108
B^2	100.16	266.77	1	100.16	266.77	3.81	7.55	0.1084	0.0404
C^2	196.31	2,792.31	1	196.31	2,792.31	7.47	78.99	0.0411	0.0003
Residual	131.42	176.75	5	26.28	35.35				
Lack of Fit	129.25	168.75	3	43.08	56.25	39.77	14.06	0.0246	0.0671
PureError	2.17	8.00	2	1.08	4.00				
Cor Total	7637.23	13,654.93	14						

[a]Values of "Prob> F" less than 0.05 indicate model terms are significant.

The ratio found value 19.74 and 15.88 is adequate signal for the validity model. Furthermore, the regression coefficient (R^2 = 0.982 and 0.987 respectively for mineralization and oxidant decay) indicates that 1.8% and 1.3% variability cannot be explained satisfactorily by the empirical model in the range of operating parameters. A large value of R^2 does not imply that the regression model is a good one. However, R^2_{adj} is preferred to be used in determining the fit of a regression model, as it does not always increase when variables are added. A good agreement has been obtained between the predicted TOC removal and PS consumption and the experimental value with R^2_{adj} of 0.952 and 0.964 respectively. The

model fitted, was expressed by comparing the experimental TOC removal and PS consumption and the predicted values, parity plots were used to estimate the accuracy of the regression model are collected in Fig.1, which indicated that the proposed model had adequate approximation to the actual value [30].

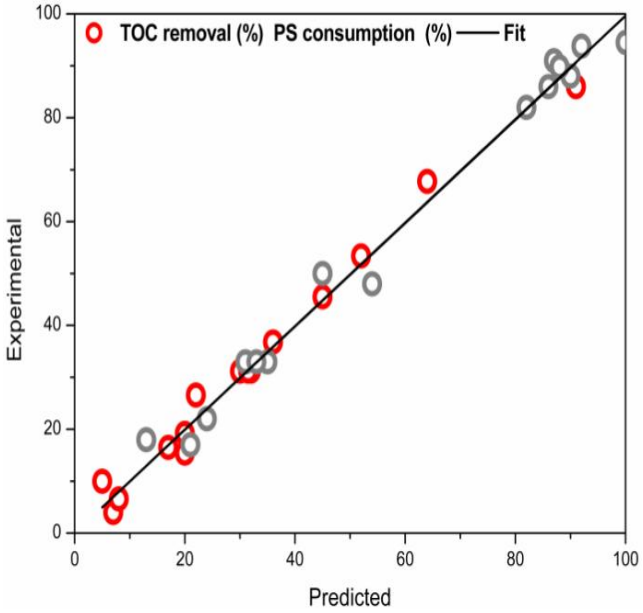

Fig.1 Predicted versus actual plot for TOC removal and PS consumption on DB3 mineralization.

3.2 Optimization design

Preliminary experiments were carried out in order to evaluate the individual process, adsorption and photocatalytic activity in absence of PS. They showed a negligible effect yielding TOC reduction lower than 2.5%. Garcia-Munóz et al.[15] suggested that the high Fe/Ti molar ratio that produces an elevated electron/holes pairs recombination, thus reducing the photocatalytic activity. Working at 67 ºC in presence of PS, TOC removal was close to 40% and around 55% in the system PS/ilmenite, corroborating the synergistic effect of combining an iron source and temperature. The heat activation (Eq. 5) and addition of ilmenite, as source of Fe(II), promotes the activation of PS to produce $SO_4^{\bullet-}$ (Eq. 6-7) [31,32].

$S_2O_8^{2-} + \text{heat} \rightarrow 2SO_4^{\bullet-}$ **(5)**

$Fe(II) + S_2O_8^{2-} \rightarrow Fe(III) + SO_4^{\bullet-} + SO_4^{2-}$ **(6)**

$Fe(II) + SO_4^{\bullet-} \rightarrow Fe(III) + SO_4^{2-}$ **(7)**

UV-LED play an important role in the ilmenite surface, due the photoreduction of Fe(III) to Fe(II). The Fe(II)/Fe(III) ratio was confirmed by XPS analysis. The Fe(II)/Fe (III) ratio was 0.66 in the natural ilmenite and was increased from 0.92 to 2.33 respectively after radiation alone and radiation in dye presence Fig.2.

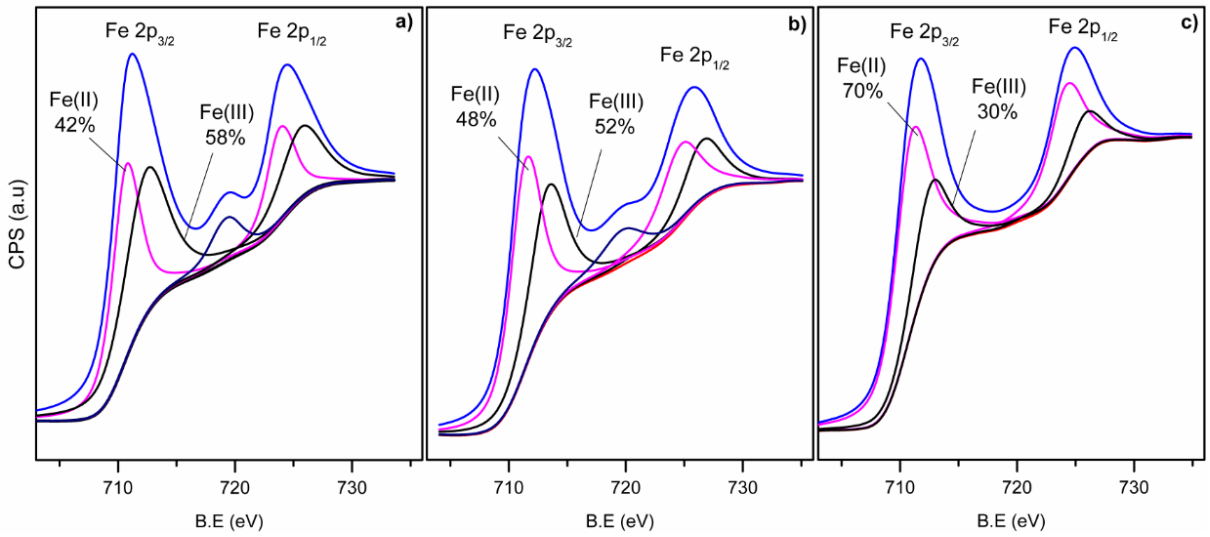

Fig. 2. XPS spectra of Fe2p for raw ilmenite, photo-reduced and photo-reduced in dye presence. Experimental Conditions: $[DB3]_0$ = 80 mg L^{-1}, $[PS]_0$ = 92%, ilmenite = 320 mg L^{-1}, pH_0 = 3, t = 180 min.

In this sense, Fig. 3 shows 3D response surface, depicting the relation of UV-LED radiation between PS dose, ilmenite concentration and reaction temperature on TOC removal and PS consumption. The non linear contour of all response surfaces suggested the interactions between each of the independent variables [33]. We used the second-order polynomial equation to optimize the process. The final predicted model can be described by the Eq. 8-9 in terms of coded values.

$$\text{TOC removal (\%)} = +31.17 + 14.50A + 8.88B + 23.38C + 4.50AB + 10.00AC + 2.25BC - 0.46A^2 - 5.21B^2 + 7.29C^2 \quad \textbf{(8)}$$

PS consumption (%) = +33 -18.50A + 17.38B +19.38C - 4.25AB + 16.25AC -15.00BC + 12.25A^2 - 8.50B^2 +27.50C^2 **(9)**

The performance of the process was optimized considering minimizing operating costs (persulfate consumption and reaction temperature) on maximum TOC removal. The resulting optimum operating conditions were 320 mg L^{-1} of ilmenite, using 92% of stoichiometric amount of PS at 67 °C. The TOC removal achieved experimentally was was slightly overestimated ($X_{TOCmodel}$: 0.92 vs X_{TOCexp}: 0.96).

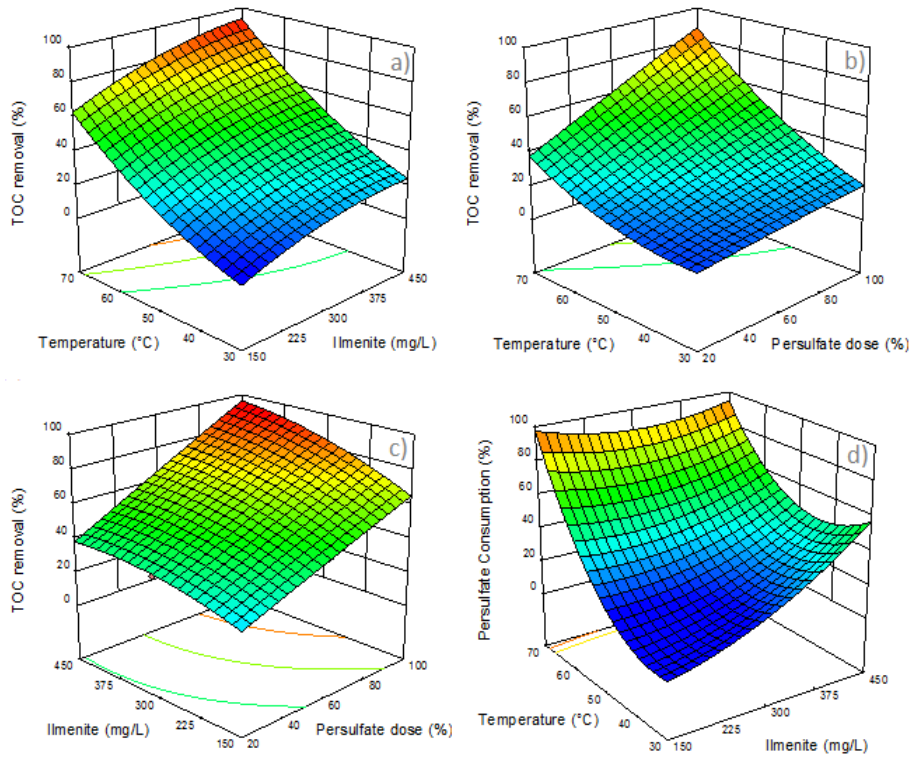

Fig. 3 Response surface plot showing interaction of ilmenite concentration and temperature (a), persulfate dose and temperature (b), persulfate dose and ilmenite concentration (c) on TOC removal and ilmenite concentration and temperature on PS consumption (d).

The expressive TOC removal efficiency by 30%, was achieved when the concentration of ilmenite increased from 150 to 450 mg L^{-1} (Fig. 3a) and approx 50% when the PS was varied between 20% and 100% of the theoretical stoichiometric dose at 67 °C

(Fig. 3b). As respects the ilmenite and PS concentration (Fig. 3c), the photoreduction of Fe(III) to Fe(II) in the reaction with high PS dose increases the $SO_4^{\bullet-}$ generation [34,35].

However, the excess of catalyst concentration (up to 320 mg L^{-1}) increases the turbidity of the DB3 solution, which reduces the penetration of light through the dye solution [36] decreasing the source of Fe(II). During the mineralization of DB3, the persulfate consumption was gradually increased as the temperature and ilmenite concentration increased (Fig. 3d). The amplitude of PS consumption varied from 20 to 90% after 180 min. To assess the PS consumption we have quantified the PS yield (Ɛ) defined as the amount of TOC converted (mg) per unit weight of PS fed (g) [37]. The theoretical maximum value of ε at complete TOC conversion when using the stoichiometric PS would be 33.5 mg TOC g^{-1} PS. The experimental ε value slightly overestimated (around 6 %) the theoretical maximum ε value, which can be justified by the contribution of oxidation processes no involving PS.

In the optimum conditions, the leached iron (measured by ICP) less than 1% of the total iron contained in the catalyst (approx. 0.8 mg L^{-1}).

The dye removal was evaluated by the normalized absorbance decrease (at 640 nm) and the change in the spectra of DB3 (200-800 nm) as a function of treatment time are represented in Fig. 4. The peak at 640 nm is responsible for the blue color and absorbance peak at 254 nm is related to the anthraquinone structure [38]. As can be observed, the absorbance at 640 nm was easily removed after 15 min treatment (about 60%). The degradation of DB3 mainly related to the destruction of chromophore structures and the increase in the absorbance peak at 254 nm can be related to the formation of persistent aromatic by-products resulting from the degradation of the dye during the early oxidation stages.

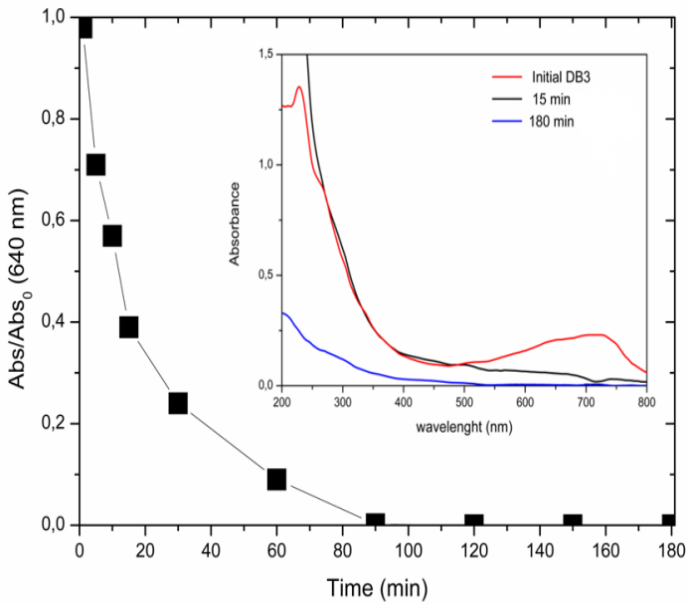

Fig. 4 UV-Vis absorption spectra of DB3 before and after degradation treatment. Inset change in the spectra of DB3 between 200-800 nm.

Intermediates products formed during the process were analyzed by GC-MS. Fig. 5 depicts the chromatograms of the reaction samples obtained throughout the experiments. After 15 min treatment, 1-amino-4-(methylamino) anthracene-9,10-dione with m/z 252 was identified, probably generated by homolytic rupture of C–N bond [39].

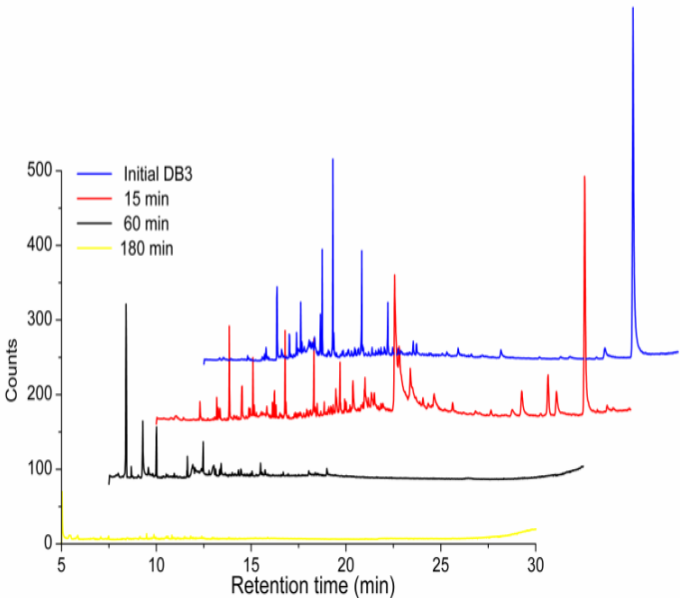

Fig. 5 GC-MS analysis of DB3 before and after experiment.

In addition, the formation of these metabolites due to incomplete mineralization of the dye increased the toxicity of the azo dye solution about 27% in relation to original DB3. Finally, these aromatic intermediates are almost mineralized. Consequently, toxicity test results showed that the acute toxicity of DB3 dye has also been reduced significantly: TU decreased from 22 to 2 for *A. fischeri* after 180 min treatment (Fig S2).

3.3. Deactivated ilmenite surface

The recovered ilmenite under the optimum experimental conditions were carried out. Negligible activity upon the third run (mineralization < 5%) was evaluated. Concerning the XPS of the O 1s and S 2p spectrum (Fig. S3) the increase in the signal intensities peaks of the deactivated catalyst was observed. Sulfur was not detectable on the fresh catalyst. Al-Shamsi and Thomson [40] detected $FeSO_4$ at a binding energy of 531.5 eV in O 1s (the peak between 529.8 and 532.3 eV correspond to the surface lattice oxygen of metal oxides, the surface hydroxyl species and the adsorbed oxygen or water [41]) and 168.6 in S 2p spectra on deactivated nZVI surface exposed to persulfate. Descostes et al. [42] showed that $FeSO_4$ and $Fe_2(SO_4)_3$ was formed at 168.95 eV. and 169 eV respectively. On the other hand, the deactivation could be attributed to the presence of iron sulfate generated on the ilmenite surface.

4. Conclusion

RSM model equations can therefore satisfactorily describe the inter-relationships between independent and dependent variables, determining the best solutions, reducing the number of tests and hence reducing the costs associated to the experiments. The combined UV-LED/ilmenite/PS show synergetic effect compared to the individual processes, achieving

DB3 mineralization around 96% under the optimum operating conditions (320 mg L^{-1} of ilmenite, using 92% of stoichiometric amount of PS at 67 °C under UV-LED radiation). In addition, the mineralization of DB3 in the UV-LED/ilmenite/persulfate system is efficient in removing the toxic properties of the dye as shown by the Aliiv*ibrio fischeri* bacteria assay.

Acknowledgment

Comunidad Autónoma de Madrid and MINECO have supported this work through projects S2013/MAE-2716 and CTQ2013-41963-R, respectively. Jefferson E. Silveira and Wendel S. Paz gratefully acknowledges the support from CAPES: Science Without Borders Program, Ministry of Education Brazil, under grant BEX-1046/13-6 and BEX-9476/13-0 respectively.

References

[1] Jo WK, Tayade RJ. Recent developments in photocatalytic dye degradation upon irradiation with energy-efficient light emitting diodes. Cuihua Xuebao/Chinese J Catal 2014;35:1781–92. doi:10.1016/S1872-2067(14)60205-9.

[2] Sen SK, Raut S, Bandyopadhyay P, Raut S. Fungal decolouration and degradation of azo dyes: A review. Fungal Biol Rev 2016;30:112–33. doi:10.1016/j.fbr.2016.06.003.

[3] Yamjala K, Nainar MS, Ramisetti NR. Methods for the analysis of azo dyes employed in food industry - A review. Food Chem 2016;192:813–24. doi:10.1016/j.foodchem.2015.07.085.

[4] Paz A, Carballo J, Pérez MJ, Domínguez JM. Biological treatment of model dyes and textile wastewaters. vol. 181. Elsevier Ltd; 2017. doi:10.1016/j.chemosphere.2017.04.046.

[5] Jegatheesan V, Pramanik BK, Chen J, Navaratna D, Chang CY, Shu L. Treatment of textile wastewater with membrane bioreactor: A critical review. Bioresour Technol 2016;204:202–12. doi:10.1016/j.biortech.2016.01.006.

[6] Brillas E, Martı CA. Applied Catalysis B : Environmental Decontamination of wastewaters containing synthetic organic dyes by electrochemical methods : A general review 2008;87:105–45. doi:10.1016/j.apcatb.2008.09.017.

[7] Almeida EJR, Corso CR. Chemosphere Comparative study of toxicity of azo dye Procion Red

MX-5B following biosorption and biodegradation treatments with the fungi Aspergillus niger and Aspergillus terreus. Chemosphere 2014;112:317–22. doi:10.1016/j.chemosphere.2014.04.060.

[8] Wang J, Ding Y, Tong S. Fe-Ag/GAC catalytic persulfate to degrade Acid Red 73. Sep Purif Technol 2017;184:365–73. doi:10.1016/j.seppur.2017.05.005.

[9] Anipsitakis GP, Dionysiou DD. Radical Generation by the Interaction of Transition Metals with Common Oxidants Radical Generation by the Interaction of Transition Metals with Common Oxidants. Environ Sci Technol 2004:3705–12. doi:10.1021/es035121o.

[10] Matzek LW, Carter KE. Activated persulfate for organic chemical degradation: A review. Chemosphere 2016;151:178–88. doi:10.1016/j.chemosphere.2016.02.055.

[11] Ghanbari F, Moradi M, Gohari F. Degradation of 2,4,6-trichlorophenol in aqueous solutions using peroxymonosulfate/activated carbon/UV process via sulfate and hydroxyl radicals. J Water Process Eng 2016;9:22–8. doi:10.1016/j.jwpe.2015.11.011.

[12] Weng CH, Tsai KL. Ultrasound and heat enhanced persulfate oxidation activated with Fe^0 aggregate for the decolorization of C.I. Direct Red 23. Ultrason Sonochem 2016;29:11–8. doi:10.1016/j.ultsonch.2015.08.012.

[13] Teel AL, Ahmad M, Watts RJ. Persulfate activation by naturally occurring trace minerals. J Hazard Mater 2011;196:153–9. doi:10.1016/j.jhazmat.2011.09.011.

[14] García-Muñoz P, Pliego G, Zazo JA, Barbero B, Bahamonde A, Casas JA. Modified ilmenite as catalyst for CWPO-Photoassisted process under LED light. Chem Eng J 2016. doi:10.1016/j.cej.2016.05.093.

[15] García-Muñoz P, Pliego G, Zazo JA, Bahamonde A, Casas JA. Ilmenite (FeTiO3) as low cost catalyst for advanced oxidation processes. J Environ Chem Eng 2016;4:542–8. doi:10.1016/j.jece.2015.11.037.

[16] Cheng M, Song W, Ma W, Chen C, Zhao J, Lin J, et al. Catalytic activity of iron species in layered clays for photodegradation of organic dyes under visible irradiation. Appl Catal B Environ 2008;77:355–63. doi:10.1016/j.apcatb.2007.08.006.

[17] Bokare AD, Choi W. Review of iron-free Fenton-like systems for activating H2O2 in advanced oxidation processes. J Hazard Mater 2014;275:121–35. doi:10.1016/j.jhazmat.2014.04.054.

[18] Zazo JA, Pliego G, García-Muñoz P, Casas JA, Rodriguez JJ. UV-LED assisted catalytic wet peroxide oxidation with a Fe(II)-Fe(III)/activated carbon catalyst. Appl Catal B Environ 2016;192:350–6. doi:10.1016/j.apcatb.2016.04.010.

[19] Kheyrandish A, Mohseni M, Taghipour F. Development of a method for the characterization and operation of UV-LED for water treatment. Water Res 2017. doi:10.1016/j.watres.2017.06.015.

[20] Tokode O, Prabhu R, Lawton LA, Robertson PKJ. The effect of pH on the photonic efficiency of the destruction of methyl orange under controlled periodic illumination with UV-LED

sources. Chem Eng J 2014;246:337–42. doi:10.1016/j.cej.2014.03.002.

[21] Rasoulifard MH, Fazli M, Eskandarian MR. Performance of the light-emitting-diodes in a continuous photoreactor for degradation of Direct Red 23 using UV-LED/S2O8 2- process. J Ind Eng Chem 2013;24:121–6. doi:10.1016/j.jiec.2014.09.018.

[22] Liang C, Huang C-F, Mohanty N, Kurakalva RM. A rapid spectrophotometric determination of persulfate anion in ISCO. Chemosphere 2008;73:1540–3. doi:10.1016/j.chemosphere.2008.08.043.

[23] Hernández-alonso MD, Mena E, Rey A, García-mu P. Applied Catalysis B : Environmental WO 3 – TiO 2 based catalysts for the simulated solar radiation assisted photocatalytic ozonation of emerging contaminants in a municipal wastewater treatment plant effluent 2014;155:274–84. doi:10.1016/j.apcatb.2014.02.035.

[24] Pliego G, Zazo J a., Blasco S, Casas J a., Rodriguez JJ. Treatment of Highly Polluted Hazardous Industrial Wastewaters by Combined Coagulation–Adsorption and High-Temperature Fenton Oxidation. Ind Eng Chem Res 2012;51:2888–96. doi:10.1021/ie202587b.

[25] Montalb??n MG, Hidalgo JM, Collado-Gonz??lez M, D??az Ba??os FG, V??llora G. Assessing chemical toxicity of ionic liquids on Vibrio fischeri: Correlation with structure and composition. Chemosphere 2016;155:405–14. doi:10.1016/j.chemosphere.2016.04.042.

[26] Acute M, Test T. Evolution of Ecotoxicity upon Fenton ' s Oxidation of Phenol in Water 2007:7164–70.

[27] Khajeh M. Application of Box-Behnken design in the optimization of a magnetic nanoparticle procedure for zinc determination in analytical samples by inductively coupled plasma optical emission spectrometry. J Hazard Mater 2009;172:385–9. doi:10.1016/j.jhazmat.2009.07.025.

[28] Kumar A, Prasad B, Mishra IM. Optimization of process parameters for acrylonitrile removal by a low-cost adsorbent using Box-Behnken design. J Hazard Mater 2008;150:174–82. doi:10.1016/j.jhazmat.2007.09.043.

[29] Prakash Maran J, Manikandan S, Thirugnanasambandham K, Vigna Nivetha C, Dinesh R. Box-Behnken design based statistical modeling for ultrasound-assisted extraction of corn silk polysaccharide. Carbohydr Polym 2013;92:604–11. doi:10.1016/j.carbpol.2012.09.020.

[30] Silveira JE, Zazo J a., Pliego G, Bidóia ED, Moraes PB. Electrochemical oxidation of landfill leachate in a flow reactor: optimization using response surface methodology. Environ Sci Pollut Res 2014;22:5831–41. doi:10.1007/s11356-014-3738-2.

[31] Silveira JE, Barreto-Rodrigues M, Cardoso TO, Pliego G, Munoz M, Zazo JA, et al. Nanoscale Fe/Ag particles activated persulfate: optimization using response surface methodology. Water Sci Technol 2017:wst2017063. doi:10.2166/wst.2017.063.

[32] Silveira JE, Cardoso TO, Barreto-Rodrigues M, Zazo JA, Casas JA. Electro activation of persulfate using iron sheet as low-cost electrode: the role of the operating conditions. Environ Technol 2017;3330:1–9. doi:10.1080/09593330.2017.1323960.

[33] Yetilmezsoy K, Demirel S, Vanderbei RJ. Response surface modeling of Pb(II) removal from aqueous solution by Pistacia vera L.: Box-Behnken experimental design. J Hazard Mater 2009;171:551–62. doi:10.1016/j.jhazmat.2009.06.035.

[34] Zhang M, Chen X, Zhou H, Murugananthan M, Zhang Y. Degradation of p-nitrophenol by heat and metal ions co-activated persulfate. Chem Eng J 2015;264:39–47. doi:10.1016/j.cej.2014.11.060.

[35] Yan J, Han L, Gao W, Xue S, Chen M. Biochar supported nanoscale zerovalent iron composite used as persulfate activator for removing trichloroethylene. Bioresour Technol 2015;175:269–74. doi:10.1016/j.biortech.2014.10.103.

[36] Nidheesh PV, Gandhimathi R, Ramesh ST. Degradation of dyes from aqueous solution by Fenton processes: A review. Environ Sci Pollut Res 2013;20:2099–132. doi:10.1007/s11356-012-1385-z.

[37] Zazo JA, Pliego G, Blasco S, Casas JA, Rodriguez JJ. Intensification of the Fenton Process by Increasing the Temperature. Ind Eng Chem Res 2011;50:866–70. doi:10.1021/ie101963k.

[38] Salazar R, Brillas E, Sirés I. Finding the best Fe2+/Cu2+ combination for the solar photoelectro-Fenton treatment of simulated wastewater containing the industrial textile dye Disperse Blue 3. Appl Catal B Environ 2012;115–116:107–16. doi:10.1016/j.apcatb.2011.12.026.

[39] Zhao HZ, Sun Y, Xu LN, Ni JR. Removal of Acid Orange 7 in simulated wastewater using a three-dimensional electrode reactor: Removal mechanisms and dye degradation pathway. Chemosphere 2010;78:46–51. doi:10.1016/j.chemosphere.2009.10.034.

[40] Al-Shamsi MA, Thomson NR. Treatment of Organic Compounds by Activated Persulfate Using Nanoscale Zerovalent Iron. Ind Eng Chem Res 2013;52:13564–71. doi:10.1021/ie400387p.

[41] Yi Q, Bu L, Shi Z, Zhou S. Epigallocatechin-3-gallate-coated Fe3O4 as a novel heterogeneous catalyst of peroxymonosulfate for diuron degradation: Performance and mechanism. Chem Eng J 2016;302:417–25. doi:10.1016/j.cej.2016.05.025.

[42] Descostes M, Mercier F, Thromat N, Beaucaire C, Gautier-Soyer M. Use of XPS in the determination of chemical environment and oxidation state of iron and sulfur samples: Constitution of a data basis in binding energies for Fe and S reference compounds and applications to the evidence of surface species of an oxidized py. Appl Surf Sci 2000;165:288–302. doi:10.1016/S0169-4332(00)00443-8.

Supplementary Material

Click here to download Supplementary Material: Supplementary Material.docx

Graphical Abstract